Mobility Limitations in TMD Monolayers: The Influence of Impurities and Remote Phonons

Shoaib Mansoori
The University of Texas at Dallas
Dallas, USA
shoaib.mansoori@utdallas.edu

Sanjay Gopalan
The University of Texas at Dallas
Dallas, USA
sanjay.gopalan@utdallas.edu

Massimo Fischetti
The University of Texas at Dallas
Dallas, USA
max.fischetti@utdallas.edu

***Abstract*—Two-dimensional (2D) monolayer transition metal dichalcogenides (TMDs) as a channel in field effect transistors (FETs) have been studied extensively due to their promise for high carrier mobility, better gate control, and decreased short channel effects. However, these promises were made by considering free-standing layers whereas in reality, the layers need to be surrounded by dielectrics. In our study, we avoid such ideality by considering a double gate geometry in which the TMD channel has a top (hBN/HfO_2) and bottom (SiO_2) dielectric. Although we might expect an enhancement of the impurity-limited mobility due to screening from high-κ dielectrics, this benefit is actually lost when we account for scattering with the hybrid interface plasmon/phonon excitations (IPPs) which is particularly strong in the presence of high-κ dielectrics. The aim of our study is to identify how 'pure' the TMD channel must be for IPP-scattering to take control of mobility. We use the well-established *ab initio* methods to calculate the band structure and bulk scattering rates and the full-band Monte Carlo method to calculate the mobility. Our results show that assuming the low-κ hBN as top-gate dielectric the crossover between IPPs and impurity scattering occurs for an impurity concentration around mid-10^{11} cm^{-2}, whereas in structures with the high-κ HfO_2 top dielectric IPPs control the mobility at all impurity concentrations. Additionally, the carrier mobility exhibits a weak dependence on temperature with impurity scattering dominating at low temperatures.**

I. Introduction

Transition metal dichalcogenides (TMDs) have gained significant attention in recent years thanks to their unique electronic and optical properties that render them promising for various applications in nanoelectronics and optoelectronics [1]–[3]. TMDs are two-dimensional materials composed of a transition metal atom sandwiched between two layers of chalcogen atoms. Examples of popular TMDs include molybdenum disulfide (MoS_2) and tungsten diselenide (WSe_2).

In order to utilize effectively TMDs in practical devices, it is crucial to understand the behavior of charge carriers in these materials. One important aspect of carrier transport is the low-field mobility. Theoretically, this has been studied extensively in the past but mainly considering free-standing layers [4]. However, in real-world applications, TMD monolayers are typically supported by an insulating substrate and may also be gated.

One such factor is the interaction of electrons with the hybrid plasmon/optical-phonons interface excitations (IPPs) [5]–[7]. These interactions can significantly impact the transport properties of TMDs, alongside scattering with bulk phonons and charged impurities. However, the combined effects of IPPs and impurities may not always align, potentially leading to conflicting results. On one hand, previous studies have demonstrated that the presence of high dielectric constant (high-κ) materials can enhance the charge-transport characteristics by increasing the dielectric screening of the impurity scattering potential [2], [17]. This improvement in screening reduces the scattering of charge carriers by impurities. On the other hand, the presence of high-κ insulators can enhance IPP scattering, which can adversely affect carrier mobility [7].

Therefore, an important question arises: to what extent do TMD monolayers need to be 'pure' for IPPs to govern the transport, and what range of impurity concentrations in high-κ materials are most effective in improving carrier mobility? Answering this question is crucial to understand the complex interplay between impurity scattering, IPP scattering, and dielectric screening in TMD-based devices.

In this paper, we aim to address these questions by investigating the influence of high-κ insulators and impurity concentrations on the low-field carrier mobility in TMD monolayers supported by insulating substrates and gated. By analyzing both experimental data [5] and theoretical models [6], we will elucidate the competing effects of impurity scattering, IPP scattering, and dielectric screening. Our findings will provide valuable insights for optimizing the design and performance of TMD-based electronic and optoelectronic devices.

II. Theoretical Model

A. The System

We consider TMD monolayers in the double gate geometry shown in Fig. 1, assuming a SiO_2 substrate and HfO_2 or hBN as examples of high- and low-κ insulators, respectively.

We use first-principles methods to compute the band structure (Quantum ESPRESSO [8]), the phonon dispersion, and the electron-phonon scattering rates (EPW [9]). We employ the dielectric-continuum approximation to deal with dielectric screening and the interactions of the electrons with ionized-impurity and IPPs. Finally, the low-field carrier mobility is obtained by using a well-established full-band Monte Carlo method to solve the Boltzmann transport equation (BTE).

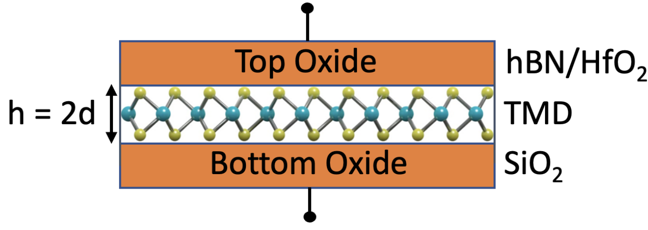

Fig. 1. Double gate device geometry assumed here.

TABLE I
INPUT PARAMETERS USED FOR QUANTUM ESPRESSO CALCULATIONS.

Parameters	
Kinetic energy (E_k) cutoff	60 Ry
Charge density cutoff	240 Ry
Ionic minimization threshold	10^{-6} Ry
Self-consistent field threshold	10^{-12} Ry
k-point mesh	12×12×1
q-point mesh	6×6×1

B. Ab initio Calculations

We use the Perdew–Burke–Ernzerhof generalized-gradient approximation (GGAPBE) [10] as the exchange-correlation functional, and the norm-conserving Vanderbilt pseudopotentials (ONCV) [11] to perform the density functional theory (DFT) calculations.

We employ the methodology outlined in Refs. [12]–[14]. To obtain the necessary input for the Monte Carlo simulations, we tabulate the band structure on a fine mesh of **k**-points (201×201×1) in reciprocal space. This mesh covers a section of the hexagonal Brillouin zone containing the irreducible triangular wedge. This fine mesh ensures an accurate determination of carrier velocity and diffusion. To reduce the stochastic noise, the zero-field mobility is extracted from the diffusion constant [12]–[14].

We obtain the phonon dispersion and the electron-phonon matrix elements from the 'Electron-Phonon Wannier' (EPW) software package [9] based on density functional perturbation theory (DFPT). Initially, these quantities are computed on a coarser **k**-mesh (12×12×1) and **q**-mesh (6×6×1) (where **q** is the phonon wave vector). Subsequently, we interpolate the data onto finer **k**- (30×30×1) and **q**-meshes (30×30×1) using maximally-localized Wannier functions, as implemented in the EPW package of the QE software suite.

C. Dielectric Screening

The presence of the top and bottom dielectrics (to which here we refer as the 'dielectric environment') induces dielectric screening of the electron-phonon interaction [7]. Performing a full DFT calculation of the electron-phonon matrix elements for the complete double-gate structure would require an impractically large supercell, making the calculations highly complex and time-consuming. Therefore, we have employed a semi-empirical approach to address this screening effect: We initially compute the electron-phonon matrix elements for a free-standing 2D layer using Quantum ESPRESSO [8] and EPW [9]. Next, considering the Hartree component as the main contribution to the scattering potential, we substitute the Green's function of the Poisson equation for the free-standing structure, as implied by DFT, with the Green's function that satisfies the boundary condition of the double-gate geometry, which includes the top and bottom insulators. This adjustment leads to a rescaling of the DFT scattering rates for the freestanding layer by the squared ratio of the Green's functions:

$$\left| \frac{\mathcal{G}^{(env)}_{Q,\omega_Q^{(\eta)}}(d,d)}{\mathcal{G}^{(\mathrm{vac})}_{Q}(d,d)} \right|^2 , \quad (1)$$

where d is the location (along the direction z normal to the layer) in the center of the layer, $\mathcal{G}^{(env)}_{Q,\omega_Q^{(\eta)}}(d,d)$ is the Green's function of the Poisson equation (expressing the potential at a location $z = d$ due to a charge also at $z = d$) satisfying the boundary condition of the dielectric environment of the double-gate geometry calculated at the wave vector Q and frequency, $\omega_Q^{(\eta)}$ of a phonon of branch η, and $\mathcal{G}^{(\mathrm{vac})}_{Q}(d,d)$ is the Green's function of the Poisson equation for a free-standing layer. The Green's function $\mathcal{G}^{(env)}_{Q,\omega_Q^{(\eta)}}(d,d)$ accounts for the presence of the 2D electron gas (2DEG) present in the TMD monolayer [7]. A detailed discussion and the assumptions made in using the scaling factor given in Eq. 1 can be found in Ref. [7].

D. Interface Plasmon-Phonon Scattering

As mentioned above, the plasma excitations of the monolayer and the optical phonons of the gate insulator, substrate, and of the polar 2D layer itself, interact giving rise to IPPs. This hybridization is very significant since it affects significantly the scattering rates, particularly for small momentum transfers, Q. Since these electron-IPP collisions cause loss of momentum of the electron gas only via the phonon-like components of each hybrid mode, we need to consider the phonon content of phonon α of each hybrid mode i, $\Phi^{(\alpha)}(\omega_Q^{(i)})$ [15], [16] for each mode i. In terms of this quantity, the amplitude $\mathcal{A}^{(\alpha)}_{Q,\omega_Q^{(i)}}$ of the scattering potential due to the phonon α (= TO1, TO2, TO3, TO4, or ZO) of each hybrid mode i is given by [7]:

$$\left|\mathcal{A}^{(\alpha)}_{Q,\omega_Q^{(i)}}\right|^2 = \Phi^{(\alpha)}(\omega_Q^{(i)})\left(1 - e^{-2Qt_{\mathrm{b}}}\right)^2 \frac{e^2\hbar\omega_Q^{(i)}}{2Q}\left|\frac{1}{\epsilon^{(\alpha,\mathrm{high})}_{\mathrm{TOT}}(Q,\omega_Q^{(i)})} - \frac{1}{\epsilon^{(\alpha,\mathrm{low})}_{\mathrm{TOT}}(Q,\omega_Q^{(i)})}\right| . \quad (2)$$

In this expression, the dielectric function of the system, $\epsilon_{\mathrm{TOT}}(Q,\omega)$, is evaluated considering full response ('low') or no response ('high') of the optical phonon α in order to isolate the contribution of each phonon to the Fröhlich-like potential given by Eq. (2). Complete details for the derivation of the above equation and its corresponding scattering rates can be found in [7].

As shown in Ref. [7], scattering with interface hybrid excitations dominates the transport and nullifies the advantage due to the dielectric screening and severely reduced the mobility of the 2D layer, below its free-standing value. As expected, it was found that the mobility decreases with an increasing dielectric constant of the top-gate insulator (from hBN to ZrO_2).

E. Impurity Scattering

We have treated scattering with charged impurities (dopants) in the TMD channel by solving Poisson Green's function for the double-gate geometry considered in our study, as described in Ref. [17] and above. The potential in the 2D layer due to a charge e located at the center of the 2D layer ($z = d$) can be written as:

$$\phi_Q^{sc}(z=d) = \frac{e^2 G_Q^{(22)}(d,d)}{1 - e^2 G_Q^{(22)}(d,d)\Pi_{2D}(Q,\omega=0)} \qquad (3)$$

where $G_Q^{(22)}(d,d)$ is the Fourier transform of the Poisson Green's function when the source charge is located at the center of the 2D layer [17], and $\Pi_{2D}(Q,\omega = 0)$ is the electronic polarizability of the 2D layer, as given by Stern [18] at zero temperature and as extended to finite temperature by Madalague [19]:

$$\Pi_{2D}(Q,\omega;T,E_\mathrm{F}) = \int_0^\infty \mathrm{d}\mu \frac{\Pi_{2D}(Q,\omega;0,\mu)}{4k_\mathrm{B}T\cosh\left(\frac{E_\mathrm{F}-\mu}{2k_\mathrm{B}T}\right)} \qquad (4)$$

where k_B is the Boltzmann constant, T the temperature, E_F the Fermi level, and $\Pi_{2D}(Q,\omega)$ is the zero temperature polarizability. Finally, the electron/ionized-impurity scattering rate for an impurity concentration N_I is given by:

$$\frac{1}{\tau^{(\mathrm{imp})}(\mathbf{k},\mathbf{n})} = \frac{2\pi}{\hbar} N_\mathrm{I} \sum_{\mathbf{k}',\mathbf{n}'} \left| \langle \mathbf{k}',\mathbf{n}' | \, \phi_Q^{(\mathrm{sc})}(\mathbf{k}-\mathbf{k}') \, | \mathbf{k},\mathbf{n} \rangle \right|^{\mathbf{2}} \times \delta(E_{\mathbf{k}'} - E_{\mathbf{k}}) \; . \qquad (5)$$

The numerical evaluation of this expression is performed by discretizing the Brillouin zone as described above and selecting energy-conserving final states with a probability given by the squared matrix elements and the final density of state calculated using the Gilat-Raubenheimer algorithm [20]. An example of the result for the $hBN/MoS_2/SiO_2$ gate stack is shown in Fig. 2.

III. Results

A. Dependence on Impurity Concentration

The calculated impurity-limited electron mobility shown in Fig. 3 confirms that expected result that the presence of a high-κ insulator improves the impurity-limited mobility (Fig. 3), as anticipated considering the effect of the stronger screening. Figure 4 (top) shows that, in the presence of the low-κ hBN IPP top insulator, IPP-scattering influences transport only when the impurity concentration is below the mid-10^{11} cm^{-2}, while in the case of a HfO_2 top-gate insulator, IPP scattering dominates at any impurity concentration (Fig. 4, bottom).

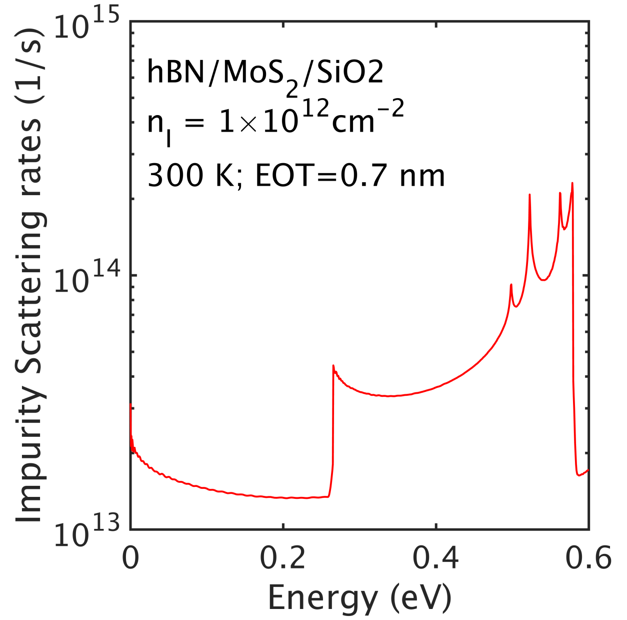

Fig. 2. Impurity scattering rates *vs.* electron kinetic energy in the $hBN/MoS_2/SiO_2$ stack calculated for an impurity concentration of 10^{12} cm^{-2} at 300 K. The insulators have been assumed to have an equivalent SiO_2 thickness of (EOT) 0.7 nm.

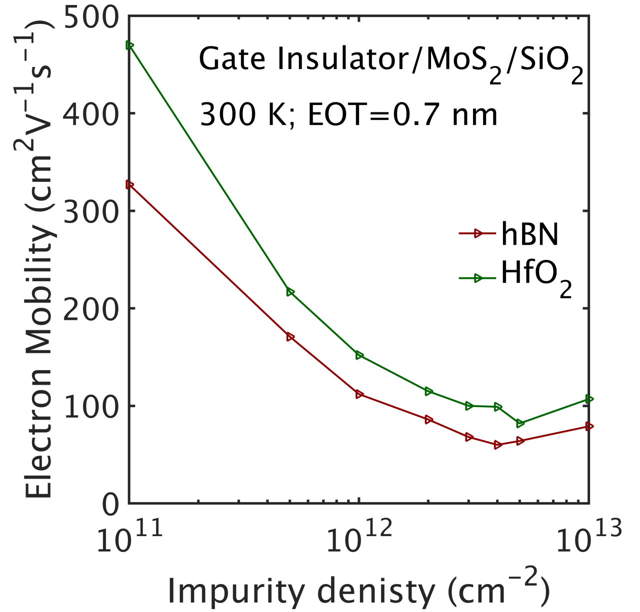

Fig. 3. Impurity-limited mobility *vs.* impurity density in the $hBN/MoS_2/SiO_2$ and $HfO_2/MoS_2/SiO_2$ stacks at 300 K.

B. Dependence on Temperature

Finally, Fig. 5 shows that at low temperatures the role of impurity scattering dominates. The monotonic increase of the impurity-limited mobility increases with increasing temperature can be explained with the Ning-Sah's decades-old argument [21] (valid at densities low enough for free-carrier

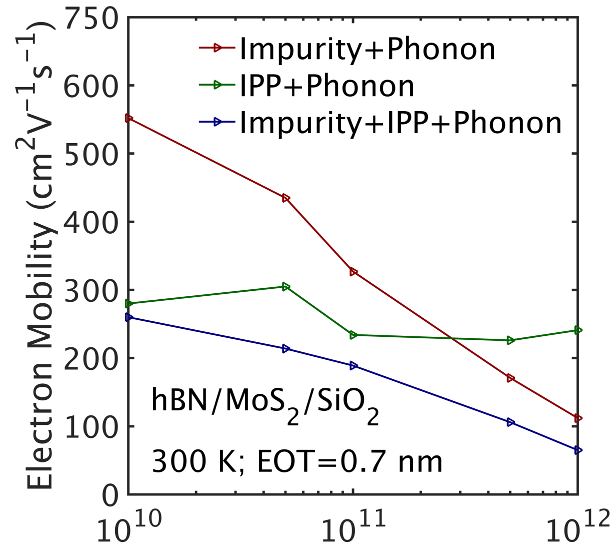

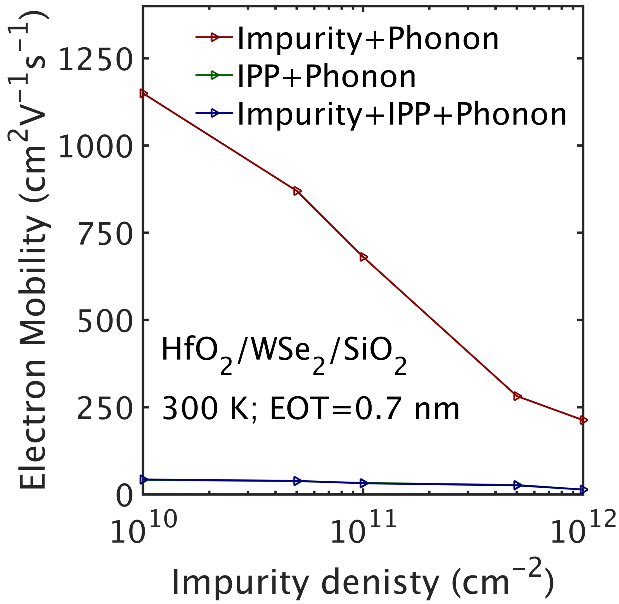

Fig. 4. Calculated electron mobility *vs.* impurity density for the hBN/MoS_2/SiO_2 (top) and HfO_2/WSe_2/SiO_2 (bottom) stacks.

screening to play a minor role) that the hotter carriers present at a high temperature suffer reduced scattering, as seen by the monotonic decrease of the scattering rates shown Fig. 2 for kinetic energies below ≈ 0.2 eV.

IV. Conclusions

We have employed *ab initio* methods and the dielectric-continuum approximation to study the effect of scattering with bulk phonons, IPPs, and charged impurities on the electron mobility in TMD monolayers in a double-gate structure. We have shown that the mobility is limited by impurity scattering at low temperatures and high impurity concentrations only when considering a low-κ top-gate insulator, such as hBN. Outside this range, IPP scattering dominates. On the contrary,

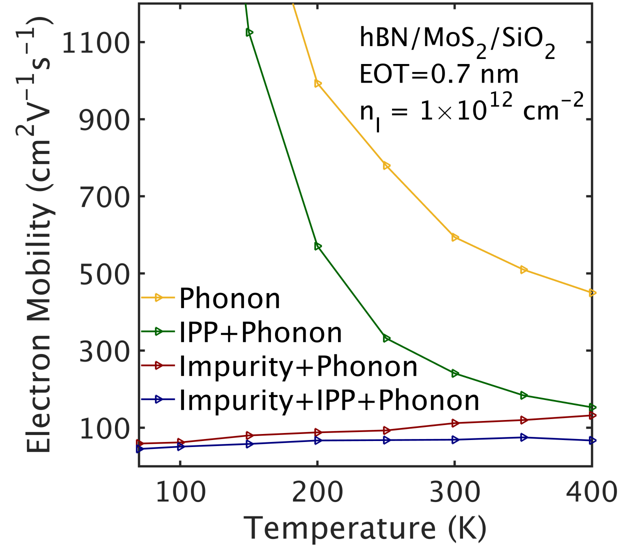

Fig. 5. Calculated electron mobility *vs.* temperature for the hBN/MoS_2/SiO_2 stack.

in the presence of a high-κ top-gate insulator, such as HfO_2, IPP scattering remains the dominant scattering process over the entire range of impurity concentrations. In both cases, the mobility exhibits a weak temperature dependence, with impurity scattering dominating at low temperatures. exhibits a weak temperature dependence

References

[1] S. Li, K. Tsukagoshi, E. Orgiu, and P. Samori, Soc. Rev. **45**, 118–151 (2016).

[2] B. Radisavljevic, A. Radenovic, J. Brivio, V. Giacometti, and A. Kis., Nat. Nanotech. **6**, 147 (2011).

[3] S. Kim *et al*, Nat. Commun. **3**, 1011 (2012).

[4] T. Gunst, T. Markussen, K. Stokbro, and M. Brandbyge, Phys. Rev. B **93**, 035414 (2013).

[5] N. Ma and D. Jena, Phys. Rev. X 4, 011043 (2014).

[6] A. Hauber and S. Fahy, Phys. Rev. B **95**, 045210 (2017).

[7] S. Gopalan, M. L. Van de Put, G. Gaddemane, and M. V,. Fischetti, Phys. Rev. Appl. **18**, 054062 (2022).

[8] P. Giannozzi S. Baroni, N. Bonini, M. Calandra, R. Car, C. Cavazzoni, D. Ceresoli, G. L. Chiarotti, M. Cococcioni, I. Dabo,

[9] S. Poncé, E. R. Margine, C. Verdi, and F. Giustino, Comp. Phys. Commun. **209**, 116 (2016).

[10] J. P. Perdew, K. Burke, M. Ernzerhof, Phys. Rev. Lett. **77**, 3865 (1996).

[11] D. Hamann, Phys. Rev. B **88**, 085117 (2013).

[12] G. Gaddemane, W. G. Vandenberghe, M. L. Van de Put, S. Chen, S. Tiwari, E. Chen, M. V. Fischetti, Phys. Rev. B **98**, 115416 (2018).

[13] G. Gaddemane, S. Gopalan, M. L. Van de Put, M. V. Fischetti, J. Comp. Electron. **20**, 49-59 (2021).

[14] G. Gaddemane, M. L. Van de Put, W. G. Vandenberghe, E. Chen, M. V. Fischetti, J. Comp. Electron. **20**, 60–69 (2021).

[15] M. V. Fischetti, D. A. Neumayer, and E. A. Cartier, J. Appl. Phys. **90**, 4587 (2001).

[16] Z.-Y. Ong and M. V. Fischetti, Phys. Rev. B **88**, 045405 (2013).

[17] Z.-Y. Ong, and M. V. Fischetti, Phys. Rev. B **86**, 121409 (2012).

[18] Frank Stern, Phys. Rev. Lett. **18**, 546 (1967).

[19] P. F. Maldague, Surf. Sci. **73**, 296 (1978).

[20] G. Gilat and L. J. Raubenheimer, Phys. Rev. **144**, 390 (1996).

[21] T. H. Ning and C. T. Sah, Phys. Rev. B **6**, 4605 (1972).